VALIDATION OF ANALYTICAL MODELS FOR THE ASSESSMENT OF BRICK-INFILLED RC FRAMES STRENGTHENED WITH FRPS

Constantine C. Spyrakos[1], Charilaos A. Maniatakis[1], Ioannis N. Psycharis[1], Eleni Smyrou[1], and Panagiotis G. Asteris[2]

[1] Laboratory for Earthquake Engineering, School of Civil Engineering, National Technical University of Athens
Iroon Polytecheiou Str., Zografou Campus, GR 15780, Athens, Greece
cspyrakos@central.ntua.gr; chamaniatakis@gmail.com; ipsych@central.ntua.gr; smiroulena@gmail.com

[2] Computational Mechanics Laboratory, School of Pedagogical & Technological Education
Heraklion GR 14121, Athens, Greece
asteris@aspete.gr

Keywords: Brick-infilled Reinforced Concrete Frames, FRP Composites, Retrofit of Structures.

Abstract. *Numerous modern seismic codes including Eurocode 8 provide rules to avoid possible adverse impact of the presence of masonry infills in concrete buildings or unbraced steel or composite structures. These adverse effects include damage of columns in contact with strong infills, reduction of the clear column height because of partial contact with masonry along height, planwise and heightwise irregularity. However, codes emphasize on the design of new structures, while little information is provided on modeling of masonry infills. Conversely, when the seismic upgrading of existing structures is performed with those methods that have received wider application in engineering practice, i.e., strengthening of columns and beams with reinforced concrete (RC) jackets or Fiber Reinforced Polymers (FRPs), construction of additional RC shear walls and construction of diagonal steel elements, any beneficial effect of masonry infills is usually ignored. The present research examines the effectiveness of strengthening existing RC frames with the application of FRP sheets on their brick-infill walls. This recently proposed method uses the advantageous mechanical properties of FRPs and is characterized by relatively low cost and ease of implementation compared to other aforementioned available retrofit schemes. A multi-strut masonry panel element is used to simulate the nonlinear response of the infill wall, while the FRP contribution to the response is modeled with a tension tie. Experimental results available in the literature for a scaled reinforced concrete frame are used to calibrate the parameters of the numerical model. Comparisons are made between the analytically and the experimentally derived results, and the effectiveness of the retrofit scheme is assessed. Also a simple method to modify the lateral stiffness of masonry infills to account for the presence of openings is addressed.*

1   INTRODUCTION

The modelling of masonry infills in reinforced concrete (RC) structures has received less attention from design codes, since non-structural masonry infills are usually considered as a beneficial second line of defence for the structure, provided that they are effectively confined by the surrounding frame and properly placed. The current Eurocode 8 [1], following this concept, does not provide detailed guidance on modelling masonry infill panels, except for the case of solid infill panels, while it provides appropriate rules to avoid possible adverse impact of the presence of masonry infills in concrete buildings or unbraced steel or composite structures. These adverse effects include [2]:

(i)   Possible damage of columns in contact with strong infills; the presence of infills is considered in the shear design of RC columns of the surrounding frame.

(ii) Reduction of the clear column height because of partial contact with masonry along height ('short column' effect); in that case, pre-emptive brittle failure of the surrounding is possible.

(iii) Plan-wise or height-wise irregularity; an asymmetric distribution of infills in plan may cause significant torsional response, while a soft or weak storey may cause an unexpected concentration of damage.

Ignoring infills in design is also attributed to the lack of ductile behaviour, their complex dynamic behaviour, the uncertainty and large variability of critical parameters, the lack of sufficient experimental data, and the difficulty in modelling many of the failure modes because of the interaction of masonry with the frame members [3].

A large number of reinforced concrete (RC) structures with masonry infills were severely damaged or even collapsed during recent earthquakes. Existing brick-infilled RC buildings often present common weaknesses attributed to their design or construction that explain their high seismic vulnerability, e.g. existence of soft first or intermediate storey, application of the strong-beam and weak-column design approach, use of low-strength concrete, and lack of adequate reinforcement detailing.

Usually, upgrading of existing RC structures is related with extensive interventions, aesthetical modifications, and significant cost or even operational interruptions. Common retrofit schemes include construction of new reinforced concrete shear walls, precast elements or steel diagonal struts, and the use of RC jackets. In this sense, the consideration of the contribution in strength and stiffness of masonry infills might be beneficial in providing a most effective retrofit scheme. The present research studies the efficiency of upgrading existing masonry-infilled RC frame structures with the use of Carbon Fibre Reinforced Polymers (CFRP). The fibre reinforced polymers are characterized by small thickness and weight, relative ease of application, resistance to environmental conditions and high strength compared to conventional materials. Their application results in significant increase in strength with very little modification of mass and stiffness; thus, slightly modifying the design seismic loads that are expected for the retrofitted structure [4-6].

Under small lateral loading, the RC frame and the infill masonry operate uniformly as a single body, while the increase of lateral load leads to a highly non-linear behaviour [7]. The contribution of infill walls to lateral stiffness depends on the type of loading and is drastically reduced under reversed cycling loading [8]. In engineering practice, infill walls are usually modelled as a combination of diagonal struts following a macro-modelling approach [9, 10] while more complex models exist that implement constitutive relations available in the literature to account for the non-linearity of the response [11-14].

In infilled RC frames with no openings, the orbits of compressive and tensile stresses follow the two diagonal paths. Therefore, the infill wall behaves as a strut in the diagonal that is

under compression, while detachment from the surrounding frame is observed at the other diagonal. The placement of CFRP along the two main diagonals allows the wall to undertake tensile stresses along the tensile diagonal, limiting the deformation of the frame and increasing the resistance to lateral loads [15, 16]. Several efforts have been made recently to understand the in-plane and out-of-plane behaviour of FRP infilled RC frames [5, 15-18] that resulted in the identification of two main failure modes for this retrofit method: (a) anchor failure; and (b) debonding. Since widespread dispersion in the mechanical characteristics of masonry is observed, the most possible accurate knowledge of these values is important for the effective application of this retrofit scheme.

The present research attempts to validate analytically the effectiveness of the FRP application on brick infilled RC frames using the experimental results of Akgüzel [19] and Özden & Akgüzel [18]. The nonlinear response of the brick infill wall is modelled applying the four node masonry panel element developed by Crisafulli [10], available in SeismoStruct [20], a fibre-based finite element software package for static and dynamic analyses, that takes into account both geometric and material nonlinearities.

2   DESCRIPTION OF SPECIMENS AND LOADING

The research of Akgüzel [19] includes experiments on five identical two-storey scaled frames named U_i (i=1, 2, …, 5), that exhibit structural shortcomings, i.e., lack of sufficient anchorage length of the longitudinal reinforcement, low concrete strength, insufficient column lap splice length and poor confinement: (1) U_1 frame was a bare frame without infills; (2) U_2 frame was identical to U_1 with brick-infills without FRP strengthening; (3) U_3 frame was identical to U_2 with CFRP sheets of inadequate bond length along the two main diagonals on both stories; (4) U_4 frame was identical to U_3 with rather sufficient bond length on the masonry surface; (5) U_5 frame was identical to U_3 and U_4 but the appropriate anchorage of the FRPs was achieved by extending the sheets outside the diagonals of the infills on the columns of the frame. All the experiments were conducted in the Structures Laboratory of Boğaziçi University. Only the first three frames U_1, U_2 and U_3 are considered in the present research.
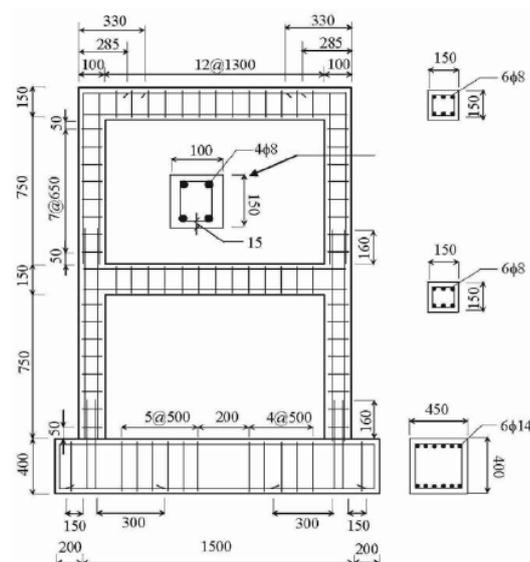

Figure 1: Bare frame U_1 tested in the Boğaziçi University, Structures Laboratory (dimensions in mm) - reproduced from [19].

The two-storey, one-bay plane frame with a 0.90 m typical storey height and 1.50 m typical bay length is shown in Fig. 1. Orthogonal sections of 100 mm × 150 mm and 150 mm × 150 mm were used for the columns and the beams, respectively, as shown in Fig. 1, with the small dimension of the columns' section being in-plane with the frame. The compressive strength of the concrete was slightly varying between the frames, with an average value of f_c = 15.4 MPa and reinforcement with yield strength f_y = 241 MPa was used for the columns and the beams. Bricks, with dimensions: 70 mm (height, put in the vertical direction), 90 mm (width) and 85 mm (length), were used for the construction of infill walls in frames U_2 to U_5. Low strength mortar was used between the brick connection and for the plaster. The CFRP sheets were applied at both sides of the masonry using epoxy resin. In all specimens, the material was applied in layers of 200 mm, in such a way that could operate along the two main diagonals of the wall. The tensile strength and the modulus of elasticity of the fibres were f_{fib} = 3500 MPa and E_{fib}=230000 MPa, respectively. The tensile strength and the modulus of elasticity of the epoxy were f_m = 30 MPa and E_m=3800 MPa, respectively. For more information on the material properties one should refer to [18, 19].

Cyclic loading was applied to the specimens in two phases: firstly, the frames were pushed under lateral cyclic forces with a triangular pattern along their height, until the first yield occurred; then, a cyclic loading phase was following till failure. The loading history for U_1 frame is shown in Fig. 2.

3   MODELING OF THE SPECIMENS

As mentioned, three types of RC frames were studied: the bare frame U_1 and two infilled frames, the un-strengthened frame U_2 and the CFRP strengthened frame U_3. The numerical models for the bare frame and the infilled ones had the same geometry with the typical section details shown in Fig. 1. The frame structure was modelled using inelastic fibre elements for the beams and the columns, which were calibrated from the experiments [19]. The steel model proposed by Menegotto and Pinto [21, 22] and the nonlinear constant confinement concrete model of Mander *et al.* [23] were applied for the reinforcement bars and the concrete, respectively.

The masonry panel element model used in the present study was originally developed by Crisafulli [10] and calibrated by Smyrou [24]. Each panel element contained six elements: two struts parallel to each diagonal that transferred the axial load between the two diagonal
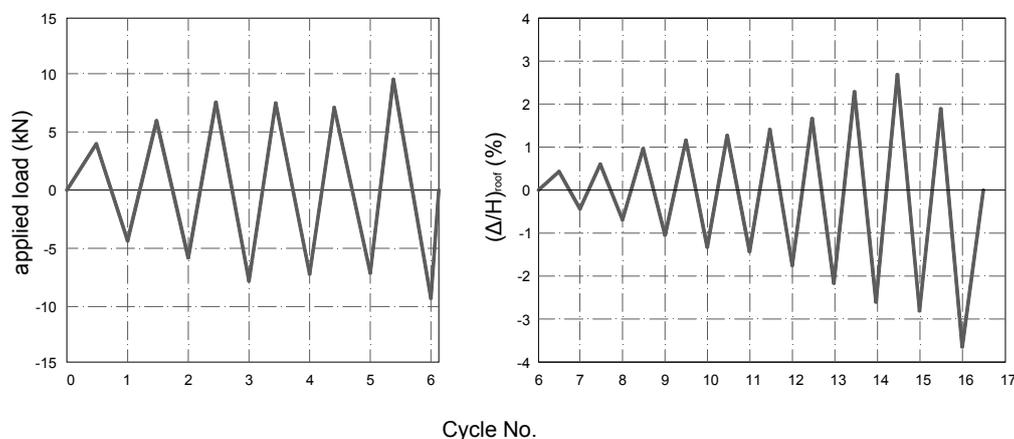

Figure2 : Loading history for cyclic analysis of the bare frame U_1 [19].

nodes and a pair of springs related to each diagonal (one for each direction of loading) that transferred the shear load from the top of the wall to the base. Each one of the latter was activated if the corresponding diagonal at which it belonged was compressed; thus its activation was directly dependent on the deformation level of the masonry.

A simple uniaxial tri-linear model that acts only under tension was used to simulate the CFRP. The main parameters that determine the response of this element are: (i) the tensile strength, f_t; (ii) the initial stiffness, E_1; (iii) the post-peak stiffness, E_2; and (iv) the specific weight, γ. The main parameters needed to describe the constitutive laws of the models implied are shown in Table 1. The selected values result from either the characteristics of the materials used for the specimens' construction [19] or the parametric analyses that follow. The range of values and the default values described in Table 1 are indicative and are based on the literature included in the development of the Seismostruct code [20]. When a value is not included in the "common range of values" column, either the range is extremely wide or there are insufficient experimental data to determine a reasonable range for this parameter. In several cases the parameter is calculated analytically, so the determination of a strict range is of no point. In the following, a brief discussion on these main parameters is made.

As discussed previously the model proposed by Crisafulli [10] uses two pairs of diagonal struts that act mainly under compression and a pair of shear springs that transfer shear loads

| Model	Parameter name	Default value in Seismostruct	Common range of values	Selected value
Concrete model - Mander *et al.* [23]	Compressive strength - f_c	30.0 MPa	15 ~ 45 MPa	15.4 MPa
	Tensile strength - f_{tc}	0.0 MPa	0.50 ~ 0.75 MPa	0.0 MPa
	Strain at peak stress - ε_c	0.002 mm/mm	0.002 ~ 0.0022 mm/mm	0.002 mm/mm
Steel model - Menegotto & Pinto [21, 22]	Modulus of elasticity - E_s	200 GPa	200 ~ 210 GPa	195 GPa
	Yield strength - f_y	500 MPa	230 ~ 650 MPa	200 MPa
	Strain hardening parameter - μ_s	0.005	0.005 ~ 0.015	0.005
	Transition curve initial shape parameter - R_0	20.0		19.0
	Transition curve shape calibrating coefficient - a_1	18.5		18.7
	Transition curve shape calibrating coefficient - a_2	0.15	0.05 ~ 0.15	0.15
Masonry Panel Model - Crisafulli [10]	Initial Young modulus - E_{mas}	1.6 GPa		1.7 GPa
	Compressive strength - f_{mas}	1 MPa		1.65 MPa
	Tensile strength - $f_{t,mas}$	0.575 MPa		0.575 MPa
	Strut Area 2 - A_2	40 %		15 %
	Strain at maximum stress - $e_{m,mas}$	0.0012 mm/mm	0.001 ~ 0.005 mm/mm	0.0014 mm/mm
	Utimate strain - $e_{u,mas}$	0.024 mm/mm		0.012 mm/mm
	Closing strain - $e_{cl,mas}$	0.003 mm/mm	0 ~ 0.003 mm/mm	0.003 mm/mm
	Strut area reduction strain – e_1	0.0006 mm/mm	0.0003 to 0.0008 mm/mm	0.0006 mm/mm
	Residual strut area strain – e_2	0.001 mm/mm	0.0006 ~ 0.016 mm/mm	0.002 mm/mm
	Shear bond strength – τ_0	0.3 MPa	0.1 ~ 1.5 MPa	0.7 MPa
	friction coefficient - μ_{mas}	0.3	0.1 ~ 1.2	1.2
	Maximum shear strength - τmax	0.6 MPa		1.2 MPa
	Starting unloading stiffness factor - γ_{un}	1.5	1.5 ~ 2.5	1.5
	Strain reloading factor - α_{ch}	0.2	0.2 ~ 0.4	0.2
	Plastic unloading stiffness factor - e_{x1}	3.0	2.0 ~ 3.0	3.0
Trilinear CFRP model	Tensile strength - f_t	3000 MPa	1900 ~ 4800 MPa	953 MPa
	Initial stiffness - E_1	300 GPa	70 ~ 700 GPa	130 GPa
	Post-peak stiffness - E_2	500 GPa		130 GPa

Table 1: Main model parameters.
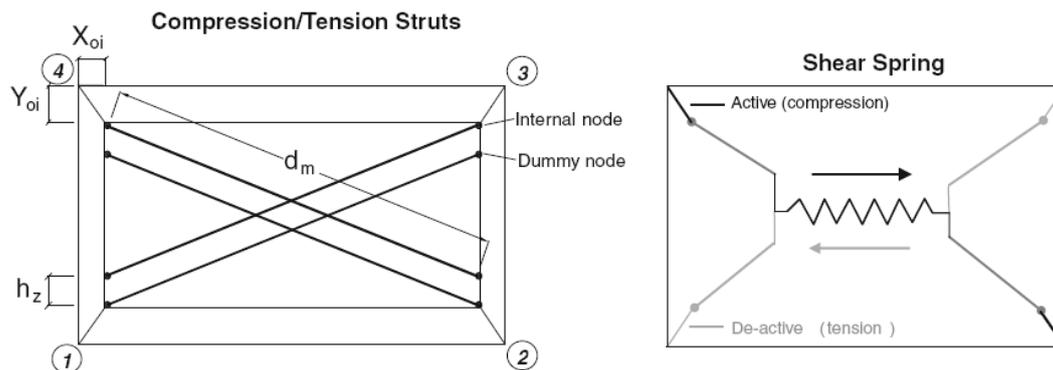
Figure 3: Four-node panel element model used in this study - reproduced from [25].

from the top to the bottom of the panel element across the diagonal under compression. Two different hysteretic rules apply for the total representation of the infill response: (i) a masonry strut hysteresis model for the diagonal struts; and (ii) a bilinear hysteresis rule for the shear springs. In Fig. 3, the two parallel struts per diagonal direction and the two shear strings (one per each diagonal direction) are shown (reproduced from Crisafulli & Carr [25]). The four dummy nodes shown in Fig. 3 are introduced to account for the contact length between the frame and the infill panel.

A relatively simple tri-linear uniaxial model is implemented for the FRP material. This model is fully described by four parameters: (i) tensile strength, f_t; initial stiffness, E_1; post-peak stiffness, E_2; and specific weight. The FRP material looses its strength very sharply upon rupture; however, a finite value is usually assigned to the post-peak stiffness E_2 to avoid numerical instability of the analyses. Since bond failure is difficult to model without the application of a more sophisticated procedure, the tensile strength f_t of the FRP was determined so that the failure occurs for the same axial deformation with the experiment; thus, in the analytical model the CFRP reaches its full tensile strength that is smaller than the original.

4 ANALYTICAL RESULTS

Two types of analyses were contacted, namely: (a) static non-linear analysis; and (b) quasi-static (cyclic) analysis, in order to: (i) compare with the experimental results; and (ii) determine "critical parameters" for the analysis.

The static non-linear analysis consisted of a Load Control phase and a subsequent Displacement Control phase and aimed to determine the capacity curve of the frames under lateral loads. A triangular load distribution was selected during the first phase, so that the load at the second floor level was always twice the load applied at the first floor. For U_1 frame, loading at the level of the second floor only was considered, as was the case during the experiment [19]. Subsequently, a Displacement Control phase followed till the desired roof displacement was reached. The load factor and the total number of steps for the two phases were different for each frame.

The second type of analysis was identical in terms of conditions and loading protocol to the experiments performed by Akgüzel [19]. A pseudo-dynamic analysis was performed, modelling the cyclic loading of the experiments. More specifically, cyclic forces were imposed at both storey levels up to yield and then displacements were imposed till failure occurred, with the exception of the bare frame where only the second floor was loaded as mentioned above. The experimental results were used to estimate the values of critical parameters of the analytical models. This assessment was made by comparing the capacity curves that resulted from the non-linear static analyses for several values of these parameters

with the corresponding backbone curves that resulted as envelopes of the lateral load–displacement hysteretic curves obtained from the experiments.

4.1 Validation of U_1 frame

The characteristic parameters of the concrete and the steel of the reinforcement were determined to account thoroughly for the response of the bare frame U_1. The lateral load–displacement curve for the cyclic test is shown in Fig. 4a, while the backbone curve was obtained after connecting the points of maximum force and displacement for each cycle.

Since the strength and the modulus of elasticity of the materials were already known [19], the following parameters had to be calibrated from the comparison with the experimental results: (i) the strain hardening parameter, μ; and (ii) the strain of concrete at peak stress, ε_c [20]. The overlap length of the longitudinal bars of the reinforcement at the base of each floor was inadequate (equal to 160 mm, twenty times the diameter of bars). Therefore, it was expected that bond slip would occur prior to yielding of the reinforcement. An accurate modelling of the bond slip would require the use of a more sophisticated model, which was out of the scope of the present research. On the other hand, the assumption that no bond slip occurs allows the reinforcement to develop its full strength, which was not the case in the experiments, thus differences from the experimental data were expected. In order to reduce the error, we assumed full bond of the rebars and reduced yield strength of the steel. It was found that a value of $f_y =$ 165 MPa resulted in an acceptable fit; thus, a reduction of f_y to ~45% of its nominal value was applied to account for the inadequate bond. Such an approximation is valid, since the primary objective of this research was to focus on the CFRP effects and on the modelling of infilled frames. A similar investigation was performed in order to determine the strain hardening parameter μ. As expected, this parameter affected the inelastic response of the frame structure and the most acceptable value resulted to be $\mu=0.00$.

In Fig. 4a, the static pushover curve for the finally selected values for all the basic parameters is compared with the curve corresponding to the experimental results. It is observed that, for the selected values of the critical parameters f_y and μ, a very satisfying match is achieved between the analytical results of static pushover analysis and the envelope of the experimental results for lateral load and displacement. The inelastic and plastic behaviour of the frame is simulated with acceptable accuracy regarding the shape and the maximum values. In the experiment, the maximum base shear was 11.16 kN and corresponded to roof displacement 17.2 mm, while the corresponding value of the analytical model was 11.07 kN at 20.3 mm roof displacement.
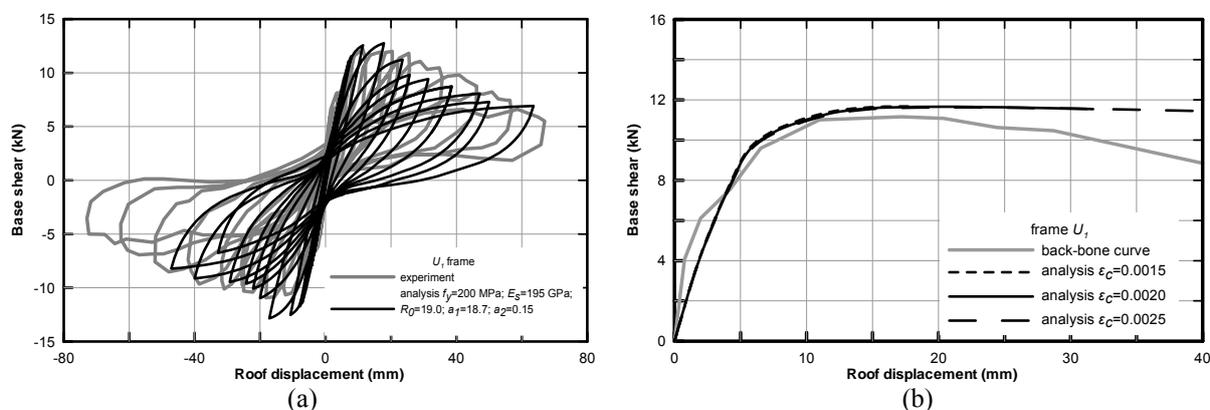

Figure 4: Comparison of the experimentally and the analytically derived load-displacement curves for U_1 frame: (a) cyclic loading, and (b) monotonic loading. The parameters used in the analytical model are; f_y = 200 MPa; E_s = 195 GPa; μ_s = 0.005; f_c = 15.40 MPa; ε_c = 0.002; R_0 = 19.0; a_1 = 18.7; a_2 = 0.15.
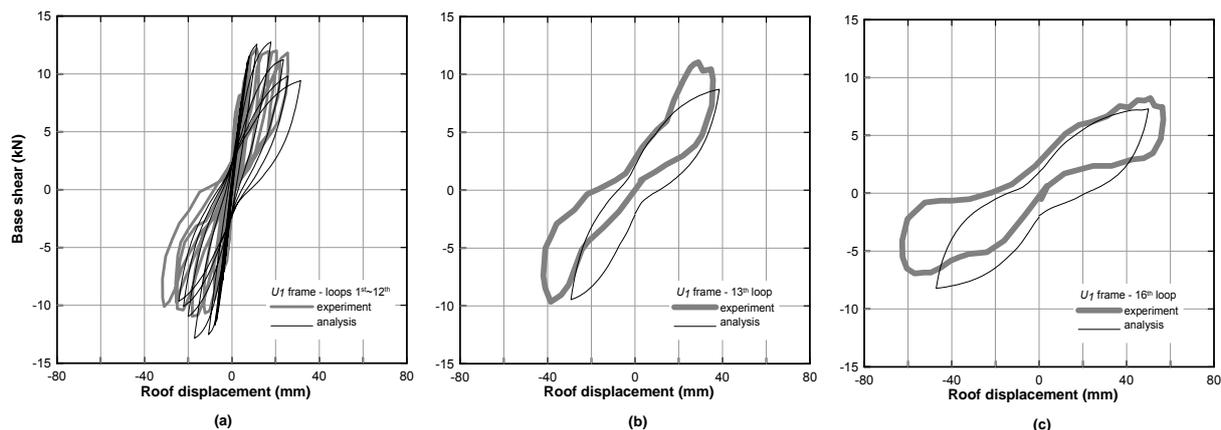
Figure 5: Comparison of the experimentally and the analytically derived load-displacement curves for U_1 frame: (a) force-displacement loops 1 to 12; (b) 13th force-displacement loop; (c) 16th force-displacement loop.

The final results of the cyclic analysis are presented in Fig. 4b and are compared with the experimentally derived curves. It is seen that the maximum base shear at each cycle and the corresponding rood displacement of the analytical model are similar to those of the experiment. In the experiment, the stiffness during unloading was decreasing progressively and the loops were narrower around the origin. This phenomenon, known as pinching, is attributed to bond slip at the overlap regions and is controlled by the parameter R and the coefficients a_1 and a_2 of the Menegotto & Pinto steel model [21]. Modifying the values of these quantities through a parametric evaluation, a better fit of the analytical and experimental results was achieved, as shown in Fig. 4b. However, a slight deviation from the analytical results still remained because full bond of the rebar was considered and the effect of the bond slip was taken under consideration with the reduction of the yield stress, as described above. This approximation slightly affected the response of the frames with infill walls, as will be shown in the following sections.

In Figs 5, the analytically derived base shear – roof displacement loops are compared with the experimental results to further confirm the applicability of the procedure. In Fig. 5a, the first twelve loops, where the maximum resistance is reached, are shown, while in Figs 5b and 5c the 13th and the 16th loops are compared, respectively, where pure inelastic response is noticed. Both the shape and the maximum values of the loops that are obtained by the analysis present acceptable accuracy.

4.2 Validation of U_2 frame

In the development of U_2 frame model, the values of the parameters for concrete and steel determined for U_1 frame were used. The applied loading protocol was similar to the one applied to the U_1 frame. The experimental results for base shear and the roof displacement for the cyclic loading and the corresponding backbone curve are shown in Fig. 6. In this case, the comparison of analytical with experimental results was used to calibrate the parameters of the Crisafulli [10] masonry panel element that was used.

For a detailed presentation of the parameters characterising the model developed by Crisafulli [10] and their effects on the overall response of masonry, the reader is referred to the work of Smyrou *et al.* [26]. Some of the parameters of the numerical model can be directly evaluated from the known geometrical characteristics of the masonry wall [19], e.g. the panel thickness. The parameters of the model that cannot be determined from the available data are the following: (i) the compressive strength, f_{mas}, and the modulus of elasticity, E_{mas}, of the masonry; (ii) the residual strut area strain, e_2; (iii) the friction coefficient of the masonry, μ_{mas};
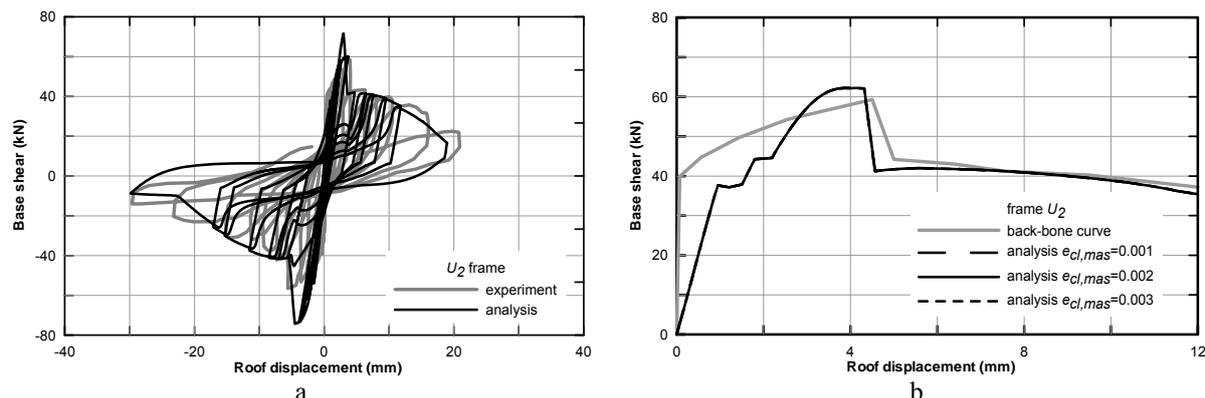
Figure 6: Comparison of the experimentally and the analytically derived load-displacement curves for U_2 frame: (a) cyclic loading, and (b) monotonic loading. The parameters used in the analytical model are; $f_{mas} = 1.65$ MPa; $E_{mas} = 1700$ MPa; $e_2 = 0.002$; $\mu_{mas} = 1.20$; $\tau_0 = 700$ kPa; $\tau_{max} = 1200$ kPa; $A_2 = 15\%$; $e_{u,mas} = 0.012$; $e_{m,mas} = 0.0014$; $e_{cl,mas} = 0.003$.

(iv) the shear bond strength τ_0 and the maximum shear strength τ_{max}; (v) the residual strut area, A_2; (vi) the ultimate strain, $e_{u,mas}$; (vii) the strain at maximum stress $e_{m,mas}$; (viii) the closing strain $e_{cl,mas}$. The basic mechanical properties, usually determined by simple test series, were not available from the experimental data [19]; thus, their determination was based also on the parametric analyses conducted, starting from reasonable assumptions.

Various combinations of f_{mas} and E_{mas} that satisfy the relationship proposed by Paulay and Priestley [27], i.e. $E_{mas} = 1000 \times f_{mas}$ have been examined in order to achieve an acceptable fit between the analytical results with the experimental data. The optimum fit was achieved for $f_{mas} = 3.5$ MPa and $E_{mas} = 3500$ MPa; however, a perfect match could not be obtained, especially regarding the displacements at which the maximum shear was attained and the horizontal branch of the pushover curve started. The calibration of the other parameters, and especially of the residual strut area strain e_2, aimed to correct the mismatch and to lead to a better assessment of the cyclic behaviour. The area of the equivalent strut strain e_2 successively reduces with the increase of the lateral displacement and the development of the cracking. The strain e_2 characterises the end of the strut section reduction, so it is related to the strain at which the frame reaches its maximum resistance.

It is observed that an increase in the deformation e_2 results in an increase in the displacement at which the frame reaches its ultimate resistance and also causes a strong amplification of the resistance itself. This happens because a larger value of e_2 delays the reduction of the strut cross section, so it amplifies the deformation and the roof displacement that correspond to the maximum resistance. Moreover, due to the lesser reduction of its cross section, the strut can resist with larger force for the same roof displacement, which explains the increased lateral resistance of the infill frame.

The final comparison of the obtained pushover curve with the backbone curve for specimen U_2 is shown in Fig. 6b. It is seen that the analytical model can capture satisfactorily the shape of the backbone curve and can describe the overall behaviour of the infill frame with acceptable accuracy for both the elastic and the inelastic ranges of deformation. In the experiment, the maximum recorded base shear was 59.64 kN and occurred at roof displacement equal to 3.74 mm. The corresponding values of the pushover analysis with the proposed model were quite similar, specifically, base shear 62.64 kN at roof displacement equal to 3.71 mm. Also, the residual resistance was similar: 40.22 kN for both the analytical and the experimental results with a small difference in the roof displacement at which the final plateau

starts. Note that the two horizontal plateaus in the ascending branch of the pushover curve of the analytical model correspond to axial failure of the tensile struts, as mentioned above.

Based on the response for various combinations of f_{mas}, E_{mas} and e_2 the finally selected values were: f_{mas} = 1.65 MPa, E_{mas} = 1700 MPa and e_2 = 0.002. The value of f_{mas} (compressive strength of the masonry) suggests very low resistance, which should not be considered as unusual for existing structures, especially those with poor mechanical properties of mortar [28]. Note that in the ascending branch of the pushover curve for the selected parameters, shown in Fig. 6b, two small horizontal plateaus are observed: the first one corresponds to base shear approximately equal to 38 kN and the second one to base shear about 45 kN. This response is attributed to failures in the diagonal struts that simulate the small tensile resistance of the masonry. When tensile failure of masonry is observed an almost instantaneous redistribution of forces takes place, i.e., the axial forces in the compressive struts and the shear loads in the frame columns suddenly increase at a nearly constant overall shear load. The first horizontal plateau corresponds to the failure of the tensile struts in the first floor and the second one to the failure of the tensile struts in the second floor.

The friction coefficient of the masonry model, μ_{mas}, the shear bond strength, τ_0, and the maximum shear strength, τ_{max}, do not significantly affect the pushover curve and the cyclic behaviour. A parametric study on the friction coefficient revealed that an increase in μ_{mas} results in trivial modification of the resistance; thus, the maximum value, μ_{mas} =1.20, was selected as most appropriate, as also suggested in the literature [27]. Similarly, the response of the frame was practically unaffected from the variation of the parameters τ_0 and τ_{max} within the limits of acceptable values; therefore, values consistent with the selected friction coefficient were considered: τ_0 = 700 kPa and τ_{max} = 1200 kPa. The residual strut area A_2 had a more significant effect on the structural response, as expected. The value A_2 = 15% was selected, which implies that the final section of the strut was equal to 15% of the original.

The ultimate strain ε_{ult} affects the response of the frame exclusively at large deformations. The value $e_{u,mas}$ = 0.012 was chosen, because it leads to results closest to the experimental data. A similar investigation on the effect of the peak strain at maximum stress $e_{m,mas}$ revealed that the ultimate lateral resistance of the frame decreases with $e_{m,mas}$, while the roof displacement that corresponds to the maximum lateral force increases. This occurs because the reduction in the strut sectional area begins before the masonry model develops its total strength. The selected value for $e_{m, mas}$ was 0.0014.
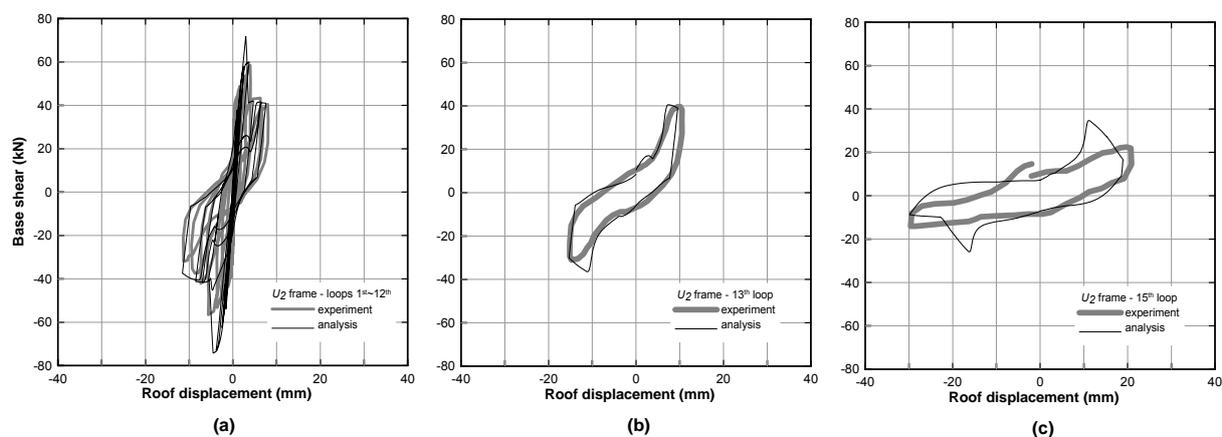

Figure 7: Comparison of the experimentally and the analytically derived load-displacement curves for U2 frame: (a) force-displacement loops 1 to 12; (b) 13th force-displacement loop; (c) 15th force-displacement loop.

Regarding the determination of the strain $e_{cl,mas}$ after which the cracks partially close allowing for compression stresses to develop, the default value of $\varepsilon_{cl,max} = 0.003$ was used, since this parameter does not seem to affect the response of the model.

Very good fit was also achieved for the cyclic loading. The maximum base shear of each cycle and the corresponding roof displacement according to the experiment and the analytical model nearly coincide, as shown in Fig. 6a. The analytical model can also predict the shape of the hysteretic loops, capturing very well the sequence of failures in the test specimen. This is more clearly depicted in Fig. 7 where individual hysteretic loops obtained analytically are compared to the experimental data. It is shown that for both nearly elastic behaviour that is identified for the first twelve loops as shown in Fig. 7a and for pure inelastic response as shown in Fig. 7b and 7c for the 13th and the 15th loop, respectively, an acceptably accurate fit is achieved by the analysis, validating the procedure applied.

4.3   Validation of U_3 frame

In the third model U_3, the parameters defined for the concrete, the steel and the masonry from the calibration of the analytical model with the experimental data for the specimens U_1 and U_2 were retained and the parametric investigation was focused on the calibration of the parameters for the FRP. Specifically, the parameters used for the frame and the infill masonry were: $f_y = 165$ MPa; $\mu = 0.00$; $\varepsilon_c = 0.00128$; $f_{mas} = 1.65$ MPa; $E_{mas} = 1700$ MPa; $e_2 = 0.002$; $\mu_{mas} = 1.20$; $\tau_0 = 700$ kPa; $\tau_{max} = 1200$ kPa; $A_2 = 15\%$; $e_{u,mas} = 0.012$; $e_{m,mas} = 0.0014$; $e_{cl,mas} = 0.003$. The loading protocol applied in specimen U_3 was similar to that for the other two specimens, consisting of a force-based phase followed by a displacement-based phase, as described earlier. In Fig. 8a, the cyclic response and its backbone envelope are shown.

The difference of specimen U_3 from specimen U_2 concerns only the strengthening with the CFRP. The parameters that define the response of the FRP are: (i) the tensile strength, f_t; (ii) the initial modulus of elasticity, E_1; and (iii) the post-peak modulus of elasticity, E_2. According to Akgüzel [19], debonding of the FRP was observed due to insufficient anchorage of CFRP sheets on the frame-wall structure.

In order to accurately account for this type of failure, and since a more complex model was not used, the selection of the parameters was made so that the FRP had smaller ultimate tensile strength than the one measured during the experiments, which was defined from the maximum axial strain developed at debonding. The modulus of elasticity was evaluated as the volumetric average of the moduli of the individual materials, i.e. the fibres and the epoxy, resulting in $f_t = 953$ MPa and $E_1 = 130000$ MPa. The post-peak modulus of elasticity was set equal to the initial modulus $E_2 = E_1$, since it was found that the response was practically unaffected by this parameter because the post-peak stiffness affected the response of the FRP at displacements greater than the displacements imposed on the test specimen. Using these values for the parameters, the comparison of the analytically predicted response with the experimental data for the FRP strengthened RC brick infilled frame are presented in Figs 8a and 8b for monotonic and cyclic loading, respectively.

Regarding the monotonic behaviour, good agreement was achieved concerning the ultimate resistance to lateral loading: in the experiment, this value was 76.23 kN and occurred at roof displacement equal to 4.87 mm, while the corresponding value of the analytical model was 71.55 kN at 4.26 mm roof displacement. However, significant discrepancy of the analytical results from the experimental data appears for large displacements, specifically for roof displacement larger than 15 mm, as shown in Fig. 8b. The difference is attributed to the different way in which the loading was implemented: in the experiment, the test specimen was partially blocked in order to follow the imposed displacement at each step [19], while the analytical model under monotonic loading was free under lateral deformations till collapse.
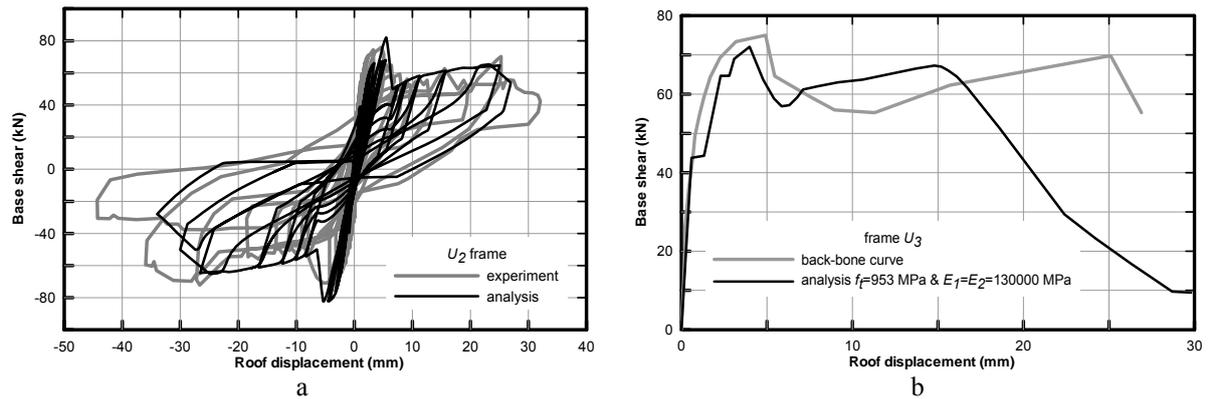
Figure 8: Comparison of the experimentally and the analytically derived load-displacement curves for U_3 frame: (a) cyclic loading, and (b) monotonic loading. The parameters used in the analytical model are; f_t = 953 MPa; E_1 = E_2 = 130000 MPa.
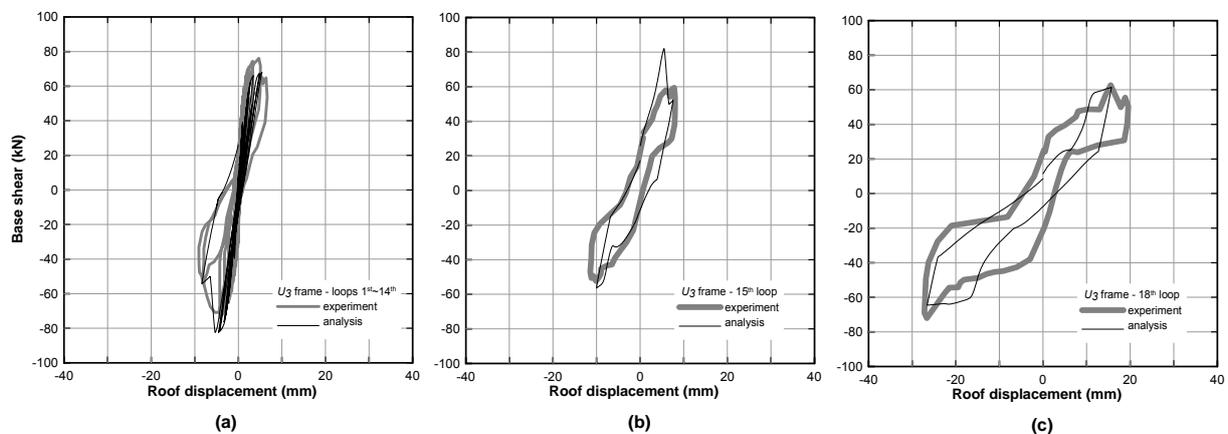

Figure 9: Comparison of the experimentally and the analytically derived load-displacement curves for U_3 frame: (a) force-displacement loops 1 to 14; (b) 15th force-displacement loop; (c) 18th force-displacement loop.

The predicted cyclic response was also very good, as evident from the comparison with the experimental data depicted in Fig. 8a. Some differences between the analytical results and the load-displacement loops obtained from the experiment, that occurred during the few last cycles, are attributed to the fact that the test the specimen was allowed to deform beyond the displacement that corresponded to the loading protocol. Thus, there was a mismatch between the assumed imposed displacements according to the loading history and the measured ones, as depicted in the cyclic loops [19]. In the numerical analysis, the loading protocol was followed, thus the displacements were smaller. Apart of this difference, the prediction of the analytical model is quite good, with the maximum base shear of each cycle and the corresponding roof displacement displaying acceptable agreement with the experimental data. This is also depicted in Fig. 9, where analytically derived base shear – roof displacement loops are compared with the experimental data. For the first fourteen loops the response is nearly elastic, as shown in Fig. 9a, and small deviations from the real behaviour are noticed. The first completely inelastic loop, which is the 15th as shown in Fig. 9b, presents smalls deviations regarding the maximum base shear. The 18th hysteretic loop is shown in Fig. 9c, where more deviations may be observed, mainly regarding the shape of the loop; however, acceptable accuracy is achieved in the maximum values of force and displacement.
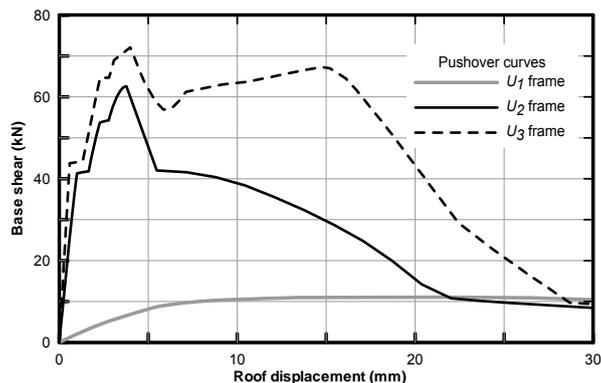
Figure 10: Load-displacement pushover curves for frames U_1, U_2 and U_3.

4.4   Comparison of the behaviour for the three frames

In order to compare the difference in strength and stiffness characteristics of the three alternative frame models U_1, U_2 and U_3, the corresponding pushover curves are drawn in Fig. 10. It is reminded that U_1 corresponds to the bare frame, U_2 was the same frame with the addition of infill masonry walls and U_3 was similar to U_2 but the infill walls were strengthened with CFRP.

It is evident that the successive upgrading of the structure, from the bare frame to a brick infilled masonry frame and to the addition of the FRP on the masonry, resulted in successive increase in the lateral resistance. The addition of the infill walls resulted in substantial increase in the stiffness, which was moderately affected by the addition of the FRP. Specifically, the maximum lateral resistance of frame U_1 was 13.75 kN, while the corresponding value for frame U_2 was 62.64 kN, demonstrating an increase of 355%. In frame U_3, the strengthening with FRP lead to further increase in the resistance by 14%, to a value of 71.55 kN. Concerning the stiffness, the initial elastic stiffness for frame U_1 was only 2.55 kN/mm, while for frames U_2 and U_3 it was 63.53 kN/mm.

Significant difference was also observed in the displacement that corresponded to the maximum base shear: frame U_1 reached its maximum resistance when the roof displacement was 18.1 mm, U_2 when it was 3.71 mm and U_3 when it was 4.26 mm.

The ductility capacity of the three frames was also significantly different. Frame U_1 showed that it could be deformed to large post-yield displacements, more than four times the yield displacement, without significant loss of strength. On the contrary, the behaviour of frame U_2 was characterized by a sharp drop of resistance after the maximum base shear was attained, evidently due to damage in the infill walls, showing a practically "brittle" response. However, the strengthening of the masonry with FRP in frame U_3 improved the response significantly, providing a relatively smooth maintenance of the resistance up to ductility around 4.0; for larger displacements, the resistance decreased sharply but remained always greater than that of U_2 without the FRP. It seems, therefore, that strengthening of the masonry with FRP improves significantly the response, as can also be seen comparing the cyclic response of frames U_2 and U_3 shown in Figs. 6a and 8a: the behaviour of U_3 was more stable and retained its resistance for a relatively large number of loops.

5   EFFECT OF OPENINGS IN THE LATERAL STIFFNESS OF INFILL WALLS

Although infill walls usually have oversized openings, recent research has mainly focused on the simple case of infill wall without openings. Research on infill walls with openings is mostly analytical, restricted to special cases, and as such cannot provide rigorous comparison to actual cases because of its focus on specific materials used and specific types of openings.

(a) 1st derived mesh

(b) 2nd derived mesh

(c) 3rd derived mesh

(d) 4th derived mesh

(e) 5th derived mesh

(f) 6th derived mesh

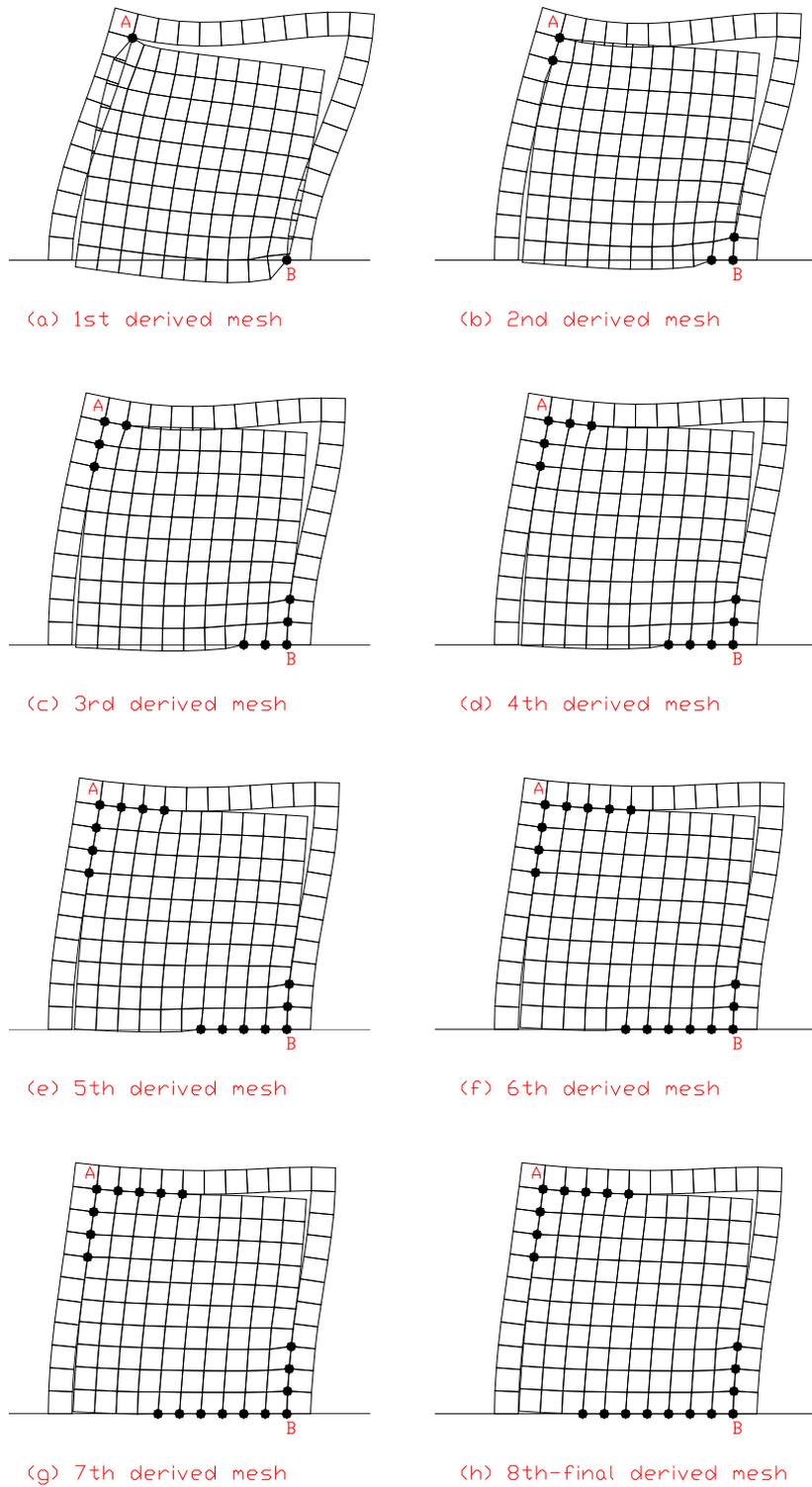(g) 7th derived mesh

(h) 8th-final derived mesh

Figure 11: Deformed meshes of a one-storey, one-bay infilled frame using the finite element technique proposed by Asteris [29, 30].

It is worth noting that the contribution of the infill wall to the frame lateral stiffness is much reduced when the structure is subjected to reverse cyclic loading, as is the case in real structures under earthquake conditions.

In order to investigate the effect of openings in the lateral stiffness of masonry infill walls, the finite element technique proposed by Asteris [29, 30] can be applied. The basic characteristic of this analysis is that the infill – frame contact lengths and the contact stresses are estimated as an integral part of the solution, and are not assumed in an ad-hoc way.

In brief, according to this technique, the infill finite element models are considered to be linked to the surrounding frame finite element models at two corner points (only), at the ends of the compressed diagonal of the infill (points A and B in Fig. 11a). Then, the nodal displacements are computed and checked whether the infill model points overlap the surrounding frame finite elements. If the answer is positive, the neighbouring points (to the previous linked) are also linked and the procedure is repeated. If the answer is negative, the procedure stops and the derived deformed mesh is the determined one (Fig. 11h).

Using this technique, analytical results are presented on the influence of the opening size on the seismic response of masonry infilled frames. Figure 12 shows the variation of the λ factor as a function of the opening percentage (opening area/infill wall area), for the case of an opening on the compressed diagonal of the infill wall (with the same aspect ratio for the opening and the infill). As expected, the increase in the opening percentage leads to a decrease in the frame's stiffness. Specifically, for an opening percentage greater than 50% the stiffness reduction factor tends to zero. The findings of the present parametric study using the finite-element method, lead to the following relationship for the infill wall stiffness reduction factor λ:

$$\lambda = 1 - 2 \cdot \alpha_w^{0.54} + \alpha_w^{1.14} \tag{1}$$

in which α_w is the infill wall opening percentage (area of opening to the area of infill wall).
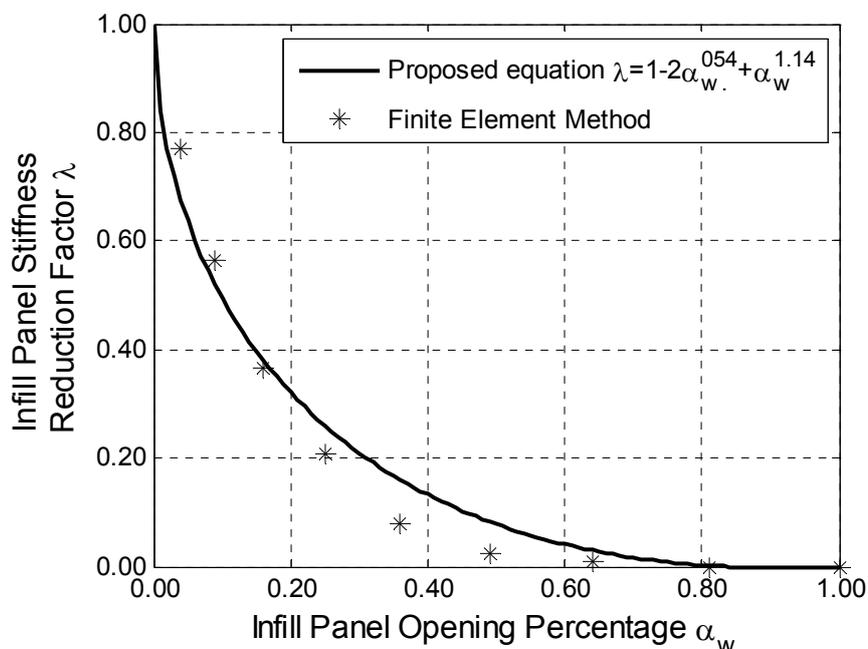

Figure 12: Infill panel stiffness reduction factor in relation to the opening percentage.

The above coefficient could be applied to find the equivalent width of a strut for the case of an infill with opening, modifying the equations of the Crisafulli model [10], which has been used in the present research.

6   DISCUSSION AND CONCLUSIONS

The research presented in this paper aims to assess the effectiveness of CFRP strengthening of brick infilled RC frame structures, typical of past design concepts. Three types of two-storey, one-bay frames were analysed with models that were validated against experimental data available in the literature [18, 19]: (i) bare frame U_1; (ii) brick infilled frame U_2; and (iii) FRP strengthened brick infilled frame U_3. The calibration of the parameters of the models was performed using experimental data for specimens that were imposed to cyclic loading and was based on the comparison of the analytical with the experimental response for the same type of loading and additionally on the comparison of analytical pushover curves with backbone curves derived from the envelopes of the cyclic response of the test specimens. For more extensive details on the material models used herein and the explanation of their critical parameters the reader is referred to [4]. In view of the present research the following conclusions can be drawn:

- The analytical model for the masonry panel element developed by Crisafulli [10] could estimate effectively the response of the brick-infilled frames that were investigated experimentally.

- Comparisons of analytically derived pushover curves with backbone curves from cyclic tests can be used to calibrate the parameters of the numerical models. Caution should be paid to the use of this method on multi-storey structures, where the results of the pushover analysis might diverge significantly from the dynamic response, being sensitive to several parameters including the pattern of the lateral load distribution, higher mode effects and special characteristics of strong ground motion [31, 32].

- Relatively small deviations were observed between the experimental and analytical results not only comparing the overall response but also comparing individual force-displacement hysteretic loops.

- The role of the masonry walls on the response is significant since they increase the resistance and the stiffness. However, the overall behaviour is rather brittle, which justifies why, in seismic design, masonry walls are not included in the assessment of the structural strength. The most critical parameters that affect the response of the masonry panel element were found to be the compressive strength f_{mas}, the modulus of elasticity E_{mas} and the residual strut area strain e_2.

- The effectiveness of the proposed retrofit scheme for brick infills was re-confirmed. Strengthening of masonry with FRP significantly increased the ductility capacity of the structure and improved its resistance. Therefore, this technique could be used to lessen the vulnerability of existing structures in earthquake-prone regions.

- The effect of openings in the response of masonry infills is an issue that deserves further analytical and experimental research. A simple method is suggested to account for the modification of lateral stiffness due to the presence of openings in masonry.

7   ACKNOWLEDGEMENTS

REFERENCES

[1]   Comité Européen de Normalisation CEN. Eurocode 8 - Design of structures for earthquake resistance, Part – 1. General rules, seismic actions and rules for Buildings. Brussels: European Committee for Standardization; 2004.

[2]   M.N. Fardis, E. Carvalho, A. Elnashai, E. Faccioli, P. Pinto, A. Plumier, *Designers' Guide to EN 1998-1 and 1998-5. Eurocode 8: Design Provisions for Earthquake Resistant Structures*, Series Editor: H. Gulvanessian, Thomas Telford Ltd, London 2005.

[3]   A.B. Mehrabi, P.B. Shing, M. Schuller, J. Noland, Experimental Evaluation of Masonry-Infilled RC Frames, *ASCE Journal of Structural Engineering*, **122**(3), 228-237, 1996.

[4]   C.C. Spyrakos, Ch.A. Maniatakis, E. Smyrou, I.N. Psycharis, FRP strengthened brick-infilled RC frames: An approach for their proper consideration in design. *Open Construction and Building Technology Journal*, **6**(SPEC. ISS. 1), 306-324, 2012.

[5]   Fédération Internationale du Béton (FIB), *Retrofitting of Concrete Structures by Externally Bonded FRPs With Emphasis on Seismic Applications*, Bulletin 35, Lausanne, Switzerland 2006.

[6]   C.C. Spyrakos, *Strengthening of Structures for Seismic Loads*, Technical Chamber of Greece Editions, 2004. (in Greek)

[7]   M. Tomaževič, *Earthquake-resistant design of masonry buildings*, Imperial College Press, 1999.

[8]   E. Vintzileou, T.P. Tassios, Seismic Behaviour and Design of Infilled R.C. Frames, *International Journal of Earthquake Engineering and Engineering Seismology*, **3**(2), 22–28, 1989.

[9]   B. Stafford-Smith, C. Carter, A Method of Analysis for Infilled Frames, *Proceedings of the Institution of Civil Engineers*, **44**(1), 31–48, 1969.

[10] F.J. Crisafulli, *Seismic Behaviour of Reinforced Concrete Structures with Masonry Infill*, Ph. D. thesis, University of Canterbury, New Zealand, 1997.

[11] J.R. Riddington, B. Stafford-Smith, Analysis of Infilled Frames Subject to Racking With Design Recommendations, *The Structural Engineer*, **55**(6), 263–268, 1977.

[12] I. Koutromanos, A. Stavridis, P.B. Shing, K. Willam, Numerical Modeling of Masonry-Infilled RC Frames Subjected to Seismic Loads, *Computers and Structures*, **89**(11-12), 1026-1037, 2011.

[13] P.G. Asteris, S.T. Antoniou, D.S. Sophianopoulos, C.Z. Chrysostomou, Mathematical Macromodeling of Infilled Frames: State of the Art, *ASCE Journal of Structural Engineering*, **137**(12), 1508-1517, 2011.

[14] I.N. Doudoumis, Finite element modelling and investigation of the behaviour of elastic infilled frames under monotonic loading, *Engineering Structures*, **29**, 1004–1024, 2007.

[15] I. Erdem, U. Akyuz, U. Ersoy, G. Ozcebe, An Experimental Study on Two Different Strengthening Techniques for RC Frames, *Engineering Structures*, **28**(13), 1843–1851, 2006.

[16] S. Altin, O. Anil, M.E. Kara, M. Kaya, An Experimental Study on Strengthening of Masonry Infilled RC Frames Using Diagonal CFRP Strips, *Composites: Part B*, **39**, 680–693, 2008.

[17] G. Ozcebe, U. Ersoy, T. Tankut, E. Erduran, R.S. Keskin, H.C. Mertol, Strengthening of Brick-Infilled RC Frames With CFRP, Ankara: SERU – Structural Engineering Research Unit, TUBITAK – METU, 2003.

[18] Ş. Özden, U. Akgüzel, CFRP Overlays in Strengthening of Frames with Column Rebar Lap Splice Problem. S.T. Wasti, G. Ozcebe eds. *Advances in Earthquake Engineering for Urban Risk Reduction*, NATO Science Series, Earth and Environmental Sciences, Springer, **66**, 455–71, 2006.

[19] U. Akgüzel, *Seismic Retrofit of Brick Infilled R/C Frames with Lap Splice Problem in Columns*, M.Sc. thesis, Department of Civil Engineering, Bogazici University, Istanbul, Turkey, 2003.

[20] SeismoSoft, SeismoStruct v5.2.5 - A Computer Program for Static and Dynamic Nonlinear Analysis of Framed Structures, 2011. [Online] Available; URL:http://www.seismosoft.com [Accessed Jan. 2012].

[21] M. Menegotto, P.E. Pinto, Method of Analysis for Cyclically Loaded R.C. Plane Frames Including Changes in Geometry and Non-Elastic Behaviour of Elements Under Combined Normal Force and Bending. International Association for Bridge and Structural Engineering. *Symposium on the Resistance and Ultimate Deformability of Structures Acted on by Well Defined Repeated Loads*, Zurich, Switzerland, 15-22, 1973.

[22] F.C. Filippou, E.P. Popov, V.V. Bertero, Modelling of R/C Joints Under Cyclic Excitations, *ASCE Journal of Structural Engineering*, **109**(11), 2666-2684, 1983.

[23] J.B. Mander, M.J.N. Priestley, R. Park, Theoretical Stress-Strain Model for Confined Concrete, *Journal of Structural Engineering*, **114**(8), 1804-1826, 1988.

[24] E. Smyrou, *Implementation and Verification of a Masonry Panel Model for Nonlinear Dynamic Analysis of Infilled RC Frames*, M.Sc. Dissertation, European School for Advanced Studies in Reduction of Seismic Risk (ROSE School), Pavia, Italy 2006. [Online] Available; www.roseschool.it [Accessed Jan. 2012].

[25] F.J. Crisafulli, A.J. Carr, Proposed Macro-Model for the Analysis of Infilled Frame Structures, *Bulletin of the New Zealand Society for Earthquake Engineering*, **40**(2), 69–77, 2007.

[26] E. Smyrou, C. Blandon, S. Antoniou, R. Pinho, F. Crisafulli, Implementation and Verification of a Masonry Panel Model for Nonlinear Dynamic Analysis of Infilled RC Frames, *Bulletin of Earthquake Engineering*, **9**(5), 1519-1534, 2011.

[27] T. Paulay, M.J.N. Priestley, *Seismic Design of Reinforced Concrete and Masonry Buildings*, John Wiley & Sons Inc., 1992.

[28] I.E. Bal, H. Crowley, R. Pinho, F.G. Gulay, Detailed Assessment of Structural Characteristics of Turkish RC Building Stock for Loss Assessment Models, *Soil Dynamics and Earthquake Engineering*, **28**(10–11), 914–932, 2008.

[29] P.G. Asteris, Lateral stiffness of brick masonry infilled plane frames, *Journal of Structural Engineering, ASCE*, **129**(8), 1071-1079, 2003.

[30] P.G. Asteris, Finite Element Micro-Modeling of Infilled Frames, *Electronic Journal of Structural Engineering*, **8**, 1-11, 2008.

[31] C.C. Spyrakos, Ch.A. Maniatakis, J. Taflambas, Evaluation of near-source seismic records based on damage potential parameters. Case study: Greece. *Soil Dynamics and Earthquake Engineering*, **28**(9), 738-753, 2008.

[32] Ch.A. Maniatakis, C.C. Spyrakos, A new methodology to determine elastic displacement spectra in the near-fault region. *Soil Dynamics and Earthquake Engineering*, **35**, 41-58, 2012.